



41th European Rotorcraft Forum
1-4 September 2015, Munich
Paper 71

Numerical Modelling of the Aerodynamic Interference between Helicopter and Ground Obstacles

Giulia Chirico ^{*}, Luigi Vigevano [†] and George N. Barakos [‡]

ABSTRACT

Helicopters are frequently operating in confined areas where the complex flowfields that develop in windy conditions may result in dangerous situations. Tools to analyse the interaction between rotorcraft wakes and ground obstacles are therefore essential. This work, within the activity of the *GARTEUR AG22 - "Forces on Obstacles in Rotor Wake"*, attempts to assess numerical models for this problem. In particular, a helicopter operating in the wake of a building, one main rotor diameter above the ground, has been analysed. Tests performed at Politecnico di Milano provide a basis for comparison to validate CFD solvers. Afterward, unsteady simulations have been performed, with and without external wind. The helicopter has been modeled as steady and unsteady actuator disk and fully resolved blade simulations have been carried out to evaluate the accuracy of those simpler models. The final goal is to find the more efficient aerodynamic model that captures the wakes interaction so that real time coupled simulations can be made. Previous studies have already proved that the wake superposition technique cannot guarantee accurate results if the helicopter is close to the obstacle. The validity of that conclusion has been investigated in this work to determine the minimum distance between helicopter and building at which minimal wake interference occurs.

NOMENCLATURE

Acronyms

AD	Actuator Disk
CFD	Computational Fluid Dynamics
HMB2	Helicopter Multi Block CFD solver
IGE	In Ground Effect
LIC	Line Integral Convolution
OGE	Out of Ground Effect
PIV	Particle Image Velocimetry
POLIMI	Politecnico di Milano
RANS	Reynolds Averaged Navier–Stokes equations
RPM	Revolutions Per Minute
UAD	Unsteady Actuator Disk
URANS	Unsteady RANS

Greek

α	normalisation factor of the UAD model [-]
ϵ	mean blade chord used in the UAD model [m]
ΔP	pressure jump of the AD model [Pa]
ΔP^*	non dimensional ΔP in the AD model [-]
η	Gaussian function used in the UAD model [-]
μ	advance ratio $\mu = \frac{U_\infty}{V_{TIP}}$ [-]
ρ_∞	free-stream density [$\frac{\text{kg}}{\text{m}^3}$]
σ	solidity of the rotor
Ψ	rotor azimuth angle [deg]

Latin	
A	rotor area [m^2]
c	blade section chord [m]
C_p	pressure coefficient $C_p = \frac{p}{\frac{1}{2}\rho_\infty V_{TIP}^2 A}$ [-]
C_T	thrust coefficient $C_t = \frac{T}{\frac{1}{2}\rho_\infty V_{TIP}^2 A}$ [-]
$C_{T,OGE}$	thrust coefficient out of ground effect [-]
f	body force in the UAD model [N]
L_x	length of the building in the x direction [m]
M_∞	free-stream Mach number [-]
M_{TIP}	tip blade Mach number [-]
N_b	number of rotor blades [-]
p	pressure [Pa]
p_∞	free-stream (far field) pressure [Pa]
R	rotor radius [m]
Re_{TIP}	blade tip Reynolds number $Re_{TIP} = \frac{V_{TIP} c}{\nu}$ [-]
Re_{ref}	reference Reynolds number $Re_{ref} = \frac{U_\infty L_x}{\nu}$ [-]
$ U $	velocity magnitude [m/s]
U_∞	free-stream velocity [m/s]
V_{IND}	rotor induced velocity [m/s]
w	vertical velocity component [m/s]

^{*}Master Student - g.chirico@liverpool.ac.uk - CFD Laboratory, School of Engineering, University of Liverpool, L69 3GH, U.K.

[†]Associate Professor - luigi.vigevano@polimi.it - Dipartimento di Scienze e Tecnologie Aeroespaziali, Politecnico di Milano, IT

[‡]Professor - g.barakos@liv.ac.uk - CFD Laboratory, School of Engineering, University of Liverpool, L69 3GH, U.K.

1. INTRODUCTION

Helicopters are increasingly employed in confined areas for search and rescue missions, urban transport or surveillance, offshore structure maintenance, etc., because of their hovering capability, low speed flying and vertical take off and landing. In these situations, the helicopter operates near ground and/or obstacles and the complex flowfields that develop, specially in windy conditions, may result in dangerous situations, as can be seen from the accident reports of the National Transportation Safety Board (NTSB) [2] or the International Helicopter Safety Team (IHST) [4]. Moreover, the pilot has to deal with a high compensatory workload, performance issues, and handling qualities of the vehicle. The rotor wake may also induce unsteady forces on the obstacles causing structural damage, and noise levels may increase discomfort to the people residing or working in the area.

Tools that allow the analysis of the helicopter-obstacle wake interaction are therefore essential and the *GARTEUR Action Group 22 - “Forces on Obstacles in Rotor Wake”* aims to generate more comprehensive experimental databases and develop a reliable and efficient numerical model of this phenomenon.

This work contributes to the GARTEUR project investigating numerically the interference between a building, simplified as a sharp parallelepiped, and a helicopter operating in its vicinity. Unsteady full-blade rotor simulations (high fidelity CFD) was first performed to validate the flow solver by means of a comparison with experimental data. Secondly, the same method was employed to evaluate the accuracy of simpler aerodynamic models. Simulations using the steady and Unsteady Actuator Disk (AD/UAD) models were carried out, while the actuator line technique was not considered because of the high computational cost. The final goal of this research was to evaluate the potential of the CFD methods to simulate the interaction at reasonable cost, finding the simplest aerodynamic model which captures the phenomenon so that efficient simulations can be performed. The other objective was to investigate the validity of the superposition technique. This is a simple uncoupled method for simulating the flowfield around the two bodies to determine the minimum distance between them where the interaction can be considered negligible.

In the past years, several studies were carried out in the direction of this paper. Quinlieven and Long [24] analysed the behavior of the rotor operating in the wake of a large structure. Flow visualizations and a Blade Element Vortex model with corrections for contraction and skewness of the wake and ground effect clearly show a development of a flow recirculation region behind the building and an alteration of the rotor downwash distribution that suggest the existence of a mutual influence between rotorcraft and ground obstacles. Polsky and Wilkinson [23] investigated a similar configuration using MILES and accounting for the atmospheric boundary layer. A hovering rotor, modeled as AD, near a hangar has been studied, analysing the effect of mesh density, different turbulence models and different inflow wind conditions. Predictions of downwash and outwash were compared with experimental data showing a good agreement when large meshes are used.

Last year, within the activity of the GARTEUR AG22, at Po-

litecnico di Milano a series of experiments have been carried out by Gibertini *et al.* [13]. The experimental setup consists of a parallelepiped, of dimensions $0.45 \text{ m} \times 0.8 \text{ m} \times 1.0 \text{ m}$, and a helicopter model, based on the MD-500, with a scaled main rotor of radius 0.375 m . The rig allows to change the horizontal distance from the obstacle, height from the ground and roll attitude of the rotor. Different positions of the helicopter with respect to the building have been tested, all without the wind. Steady (average values) pressures on the obstacle walls have been measured and PIV flow field surveys, on the building symmetry plane ahead of the front face, have been carried out.

An other experimental investigation with a small scale helicopter in ground effect has been performed by Paquet *et al.* [22] to develop the formulation of the aerodynamic forces in non uniform flows. The balance measurements allowed to propose an empirical formulation of the ratio between the rotor thrust IGE and OGE which accounts for the value of the thrust coefficient. Smoke visualisations have been also carried out to measure trajectories and convection velocities of the tip vortices.

An other configuration has been studied in the literature: the helicopter in the vicinity of a “well-shaped” object. Lusiak *et al.* [18], for example, analysed rotor and fuselage loading, air flow and flying qualities of the helicopter by means of RANS computations using the AD method. Configurations with simpler geometries have also been investigated using a complete model of the helicopter with a finite element model based on the Galerkin method for the blades and a panel method for the fuselage. The results clearly show a very high asymmetry in the rotor loading and, in some cases, the presence of vortical structures similar to a vortex ring or a horseshoe vortex which can change significantly the rotor loading. It was also estimated a drop of the thrust and an increase of the required power of about 20%.

All these studies already prove that the interaction with ground obstacles may considerably affect the dynamics of the helicopter leading to dangerous situations. Our knowledge of the phenomenon, however, is not complete and a deeper investigation is needed to guarantee the safety of helicopter operations. These are the reasons behind the creation of the GARTEUR AG22.

2. CFD FLOW SOLVER HMB2 AND AERODYNAMIC MODELS

All calculations were performed using the parallel structured CFD solver HMB2 (Helicopter Multi Block) [7, 31] of the University of Liverpool.

HMB2 solves the dimensionless 3D Navier-Stokes equations in integral form using the Arbitrary Lagrangian Eulerian (ALE) formulation for time-dependent domains with moving boundaries:

$$\vec{S} = \frac{d}{dt} \int_{V(t)} \vec{w} dV + \int_{\partial V(t)} (\vec{F}_i(\vec{w}) - \vec{F}_v(\vec{w})) \cdot \vec{n} dS \quad (1)$$

where $V(t)$ is the time dependent control volume, $\partial V(t)$ its boundary, \mathbf{W} the vector of the conservative variables

$(\rho, \rho u, \rho v, \rho w, \rho E)^T$ and \mathbf{F}_i and \mathbf{F}_v the inviscid and viscous fluxes.

The viscous stress tensor is usually approximated in HMB2 using the Boussinesq hypothesis [9]. Different turbulence models have been implemented into the flow solver: one equation models of the Spalart-Allmaras family [28, 29] and two equations models of $k - \omega$ family [19, 20, 34]. Algebraic Reynolds stress models are also available.

The Navier-Stokes equations are discretised, on the multi-block grid, using a cell-centered finite volume approach. A curvilinear co-ordinate system is adopted to simplify the formulation of the discretised terms, since body-conforming grids are adopted. The system of equations that has to be solved is then:

$$\frac{d}{dt} (\mathbf{W}_{i,j,k} \mathcal{V}_{i,j,k}) + \mathbf{R}_{i,j,k} = 0 \quad (2)$$

where $\mathcal{W}_{i,j,k}$ is the vector of conserved variables in each cell, $\mathcal{V}_{i,j,k}$ denotes its volume and $\mathbf{R}_{i,j,k}$ represents the flux residual.

Osher's upwind scheme [21] is used to resolve the convective fluxes for its robustness, accuracy and stability properties. The Monotone Upstream-centered Schemes for Conservation Laws (MUSCL) variable extrapolation method [33] is employed in conjunction to formally provide second-order accuracy. The van Albada limiter [32] is also applied to remove any spurious oscillations across shock waves. The integration in time is performed with an implicit dual-time method to achieve fast convergence. The linear system is solved using a Krylov subspace algorithm, the generalised conjugate gradient method, with a block incomplete lower-upper (BILU) [6] factorisation as a pre-conditioner.

Several low-Mach number schemes have been implemented in HMB2 to limit the loss of accuracy and round-off errors caused by the great disparity between convective and acoustic wave speeds in low-speed flows. In this work, in particular, the standard Roe scheme modified with the explicit Low-Mach method developed by Rieper [25] has been used.

Boundary conditions are set by using ghost cells on the exterior of the computational domain.

To obtain an efficient parallel method based on domain decomposition, different methods are applied to the flow solver [16] and the Message Passing Interface MPI tool is used for the communication between the processors.

Regarding the aerodynamic methods to model the rotor, there are two different approaches that can be used in CFD. The higher fidelity method models the blade with a discretisation of their geometry on the computational grid. The sliding planes technique [30] was used to allow the communication between the moving rotor grid and the fixed background. The other approach is the generalised AD method [17] which represents the blades by a disc that exerts a force on the flow and acts as a momentum source/sink. The model provides useful information about dynamic inflow and turbulent wake states occurring for heavily loaded rotors but details such as unsteady loading on the individual blades, the root and the tip blades vortices and blade boundary layer are not modeled. The method therefore provides a good estimate of the performance but, regarding the wake, only the two super-vortices are represented. To overcome the limits of the AD

model, in the actuator line technique [27] blades are represented by lines, instead of a disc, along which body forces are distributed radially. At every time step of the unsteady simulation, the local flow field and local angles of attack are computed from the movement of the blades. With tabulated airfoil data, the force per spanwise unit length is then derived using a blade-element approach. In this way a more realistic solution of the near wake is possible but the computational cost is significantly higher.

A hybrid technique, the Unsteady Actuator Disk, has also been developed. The aim was to represent the blade passing effect avoiding the complexity of the actuator line technique and the use of look-up tables for the aerodynamics. In this method, the load of the simpler AD model (momentum source) is applied to the disk with a “prescribed shape” which is rotating with the blades.

A description of the AD and UAD models implementation in the HMB2 flow solver is given below. It should be noticed that HMB2 is able to localise the computational cells which belong to the disk taking as input its radius, thickness, root cut-out dimension, position and attitude (tilt and roll). Therefore, to place the disk in the computational domain, a physical surface in the mesh is not needed.

Actuator Disk

The implementation of the AD concept requires only the addition of source terms to the momentum and energy equations to impose the pressure jump ΔP across the rotor disk which depends on the thrust coefficient C_T and on the advance ratio μ . The flowfield around the blades is not resolved and no computational cost is added to the Navier-Stokes equations. If a uniform model is considered, the ΔP in non-dimensional form is:

$$\Delta P^* = \frac{T}{\rho_\infty U_\infty^2 A} = \frac{C_{T,USA}}{\mu^2}. \quad (3)$$

In forward flight the rotor load distribution is not uniform and a more accurate model is needed. In HMB2 the Shaidakov model [26] has therefore been implemented. In this model the source term is function of the azimuth angle Ψ :

$$\Delta P^* = P_0 + P_{1S} \sin(\Psi) + P_{2C} \cos(2\Psi), \quad (4)$$

where the coefficients P_0 , P_{1S} and P_{2C} depend on rotor radius, attitude and thrust coefficient. Figure 1 shows the pressure jump distribution for the non uniform AD model. In Figure 2 the downwash distribution on the rotor disk plane is represented, for a typical forward flight condition, for both models.

Unsteady Actuator Disk

To introduce rotational effect of the blades and describe in more detail the rotor wake the UAD model has been implemented in HMB2. A Gaussian function η is used to shape the rotor load on the computational cells that belongs to the fictitious blade.

The source term on the momentum equation f in this case is therefore in the form:

$$f = \sum_{i=1}^N \left(\frac{A_i \Delta P}{\sqrt{\pi} \sigma} \eta_i \alpha \right), \quad (5)$$

where N the number of cells belonging to the actuator disk and A_i the cell area. ΔP is the pressure jump of the actuator disk from the Momentum Theory. The solidity σ of the fictitious rotor is determined assuming that the planform of the blades is triangular until half of the rotor radius, to avoid root problems, and rectangular afterwards.

The contribution of the Gaussian distribution η of each blade to the considered cell of the AD is defined as:

$$\eta_i = \sum_{j=1}^{N_b} \exp\left(-\frac{|s_j|^2}{\epsilon^2}\right), \quad (6)$$

where N_b is the number of blades, ϵ is the blade's mean aerodynamic chord and $|s_j|$ is the arc between the cell center and the actuator line.

To guarantee that the total thrust is the same of the correspondent AD, the factor α is used to normalise the source term at each time step:

$$\alpha = \frac{A}{\sum_{i=1}^N (\eta_i A_i)}. \quad (7)$$

Thus, the cell distribution on the grid does not influence the global effect of the rotor disk.

Weighting in this way the effect of each point of the actuator disk, the presence of the blades is accounted for. Figure 3 presents an example of the disk loading and the downwash distribution at different time steps of the unsteady simulation. Figure 4 shows a visualisation of the wake of the UAD via isosurface of Q criterion [15]. It can be seen that the blades vortices are represented.

3. INVESTIGATION OF THE INTERACTION HELICOPTER - OBSTACLE

Test Cases

Since the experiments of Gibertini *et al.* at POLIMI [13] have been used for a comparison, the dimensions of the helicopter and the building considered are equal to those of the wind tunnel models. The main rotor of the helicopter has a radius $R = 375$ mm. The 4 blades are rectangular, untwisted and untapered with a chord $c = 32$ mm, NACA 0012 airfoil and a collective pitch fixed to 10° . A blade root cut-out equal to the 15% of the radius has been assumed. A simplified geometry of the hub has also been reproduced. The angular velocity was equal to 2480 RPM, which corresponds to $M_{TIP} = 0.286$ and $Re_{TIP} = 214000$. The tail rotor, as in the wind tunnel tests, is not represented. In simulations with fuselage, a ROBIN fuselage (ROtor-Body INteraction) [8] was used, properly scaled to have the same blockage effect of the one of the experiments. The considered obstacle, which represents a standard building, is a simple parallelepiped with sharp edges and dimensions of 800 mm in the wind direction, 1000 mm in the transversal direction and height of 450 mm. The dimensions of the obstacle are then comparable with the rotor diameter.

To validate the flow solver, full-blades simulations in hover without wind were first performed. Secondly, simulations with external wind were carried out. The rotor was modeled as AD or UAD; full-blades simulations were also computed to evaluate the accuracy of the AD methods. Two advance

ratios have been considered: $\mu = 0.05$ and $\mu = 0.15$. For a typical helicopter with a $M_{TIP} = 0.6$, these correspond to a wind velocity around $U_\infty = 10.21$ m/s and 30.63 m/s respectively. The first wind speed, for example, occurs on average once every 5 days in Liverpool [5], the second condition is more typical of an off-shore scenario. Since the same M_{TIP} and Re_{TIP} of [13] were used, the two advance ratios result in $M_\infty = 0.0143$, $Re_{ref} = 334375$ in the first case, and $M_\infty = 0.0429$, $Re_{ref} = 1003125$ in the second. A low-Mach number correction [25] has been therefore employed in all CFD simulations.

Because of the computational cost, it was decided to perform only RANS and URANS computations, using the $k-\omega$ [34] turbulence model to close the equations. Preliminary investigations about the isolated building using different turbulence models shown that the $k-\omega$ can capture the main characteristics of flowfield with the accuracy requested to study the wakes interaction in the coupled problem. All unsteady simulations were performed with a resolution of 1 degree for every main rotor revolution, so 360 steps were resolved.

Computational Grids

The computational domain is a simple parallelepiped and the final simulations preserve the real dimensions of the large chamber of the wind tunnel in Milan. In this way, no wall effects are expected and the rotor and building wakes can develop completely. The reference system has the xz plane aligned with the mid-span plane of the building model and the xy plane aligned with the floor; the origin of the axis is located on the floor at the mid-span of the building front face (see Figure 5 (b)). The boundary conditions, see Figure 5 (a), are then set as follows: on the roof and the lateral walls, as well as on the inflow and the outflow surfaces, farfield conditions can be applied because of the distance of the building and the rotor with respect to the boundaries; for the floor, a z symmetry plane boundary condition has been chosen, because we are not interested to the boundary layer here; for the building and the helicopter (blades, hub and, if it is present, the fuselage), a solid wall condition is selected.

All grids are structured multi-block and have been generated using the ICEM Hexa tool of ANSYS [1]. Details of each grid are reported in Figure 5 and Tables 1 and 2. The sliding plane technique [30] has been used to allow the rotor rotation in the case of simulations with fully-resolved blades (see Figure 5 (d)) and to allow two different mesh densities in the external part of the domain and in the region where the wakes develop (see Figure 5 (c)). This also allowed to use the same grid, in the region of the building, for the simulations with the actuator disk and those with the blades (see Table 1) to limit the differences in the results because of the different grids. For the same reason the mesh density around the rotor and the AD in the two grids (G-b and G-e of Table 2) was kept similar. Finally, the CHIMERA technique [14] has been used together with the former in the simulations with the complete helicopter (see Figure 5 (f)).

CFD Validation

The wind tunnel tests performed at POLIMI [13] allow a comparison of the numerical results with resolved blades (highest fidelity CFD method) with the experimental data. In particular, the test case 5.2 of [13] has been selected: the helicopter is in hover on the symmetry plane of the building at one diameter above the ground, the rotor center laying exactly on the building edge (Rotor position = [0.0, 0.0, 2R], corresponding to a distance of 0.8R from the building roof).

The global flowfield that develops in this configuration is visualised in Figure 6 via Linear Integral Convolution (LIC) [10]. The interaction of the rotor wakes with the building is clearly visible. The presence of the latter deforms the “normal” IGE rotor wake and a recirculation region exists around the building. The rotor loading shows a strong asymmetry, thus the helicopter is not trimmed. Simulations including a trimmer model are part of future work. Finally, from the analysis of the thrust coefficient, we can also observe the partial ground effect produced by the building on the helicopter. As expected and confirmed by the experiments of Gibertini *et al.* [13], the additional thrust is proportional to the area that is direct under the rotor (see Table 3).

The comparison is focused on the pressure coefficient C_p on the building and on the flowfield characteristics behind it, exploiting pressure taps and PIV measurements of POLIMI. The pressure coefficient in [13] is nondimensionalised using the rotor induced velocity V_{IND} computed according to the Momentum Theory [17]:

$$C_p = \frac{p - p_\infty}{\frac{1}{2}\rho V_{IND}^2}, \quad (8)$$

$$V_{IND} = V_{TIP} \sqrt{\frac{C_{t,OGE}}{4}}. \quad (9)$$

Since the geometry of hub and blade tip were simplified (see Figure 5 (e)) and the fuselage not represented, it was expected that the “numerical” rotor would not have the same performance of the wind tunnel model. No attempt was made to trim the rotor to achieve the same thrust. A steady simulation of the isolated rotor in OGE was therefore first carried out to quantify the difference. In particular, only one blade, at 5R above the ground, was considered and periodic boundary conditions were applied. A Froude boundary condition was used for the far-field. The resulting thrust coefficient was $C_{t,OGE} = 0.0107$ and the correspondent induced velocity $V_{IND} = 7.12$ m/s. It can be noticed that the ratio $\frac{C_{t,IGE}}{C_{t,OGE}}$ is in good agreement with the data of Fradenburgh [12]. The lower performance of the “numerical” rotor (see Table 4) can be explained by the absence of the fuselage, as the balance of the experiment is nested inside it and thus the blockage effect is accounted for.

Figure 7 shows the pressure coefficient distribution on the building, averaged over the last full rotor revolution. In Figure 8 the comparison for the top face of the building is reported. An overall good agreement between CFD and experiment can be seen regarding the top and the front faces of the building, while regarding the lateral faces a large difference has to be registered. The asymmetry in the experimental results is difficult to explain and is not captured by the CFD simulation. This aspect, therefore, should be investigated in more detail.

Numerical simulations with the full helicopter model (grid G6, see Table 1) are planned to see if this effect is related to the presence of the fuselage.

Besides, a global agreement with the PIV results (see Figure 9) can be also seen. The CFD captures the velocity distribution and the flowfield structures observed during the wind tunnel tests. It should remember the significant unsteadiness of the phenomenon. Regarding the averaged flowfield however, the position of the vortex core in the recirculation zone is captured quite well.

Comparison between Different Aerodynamic Methods

To investigate in detail the phenomenon of the wakes interaction between helicopter and ground obstacles, unsteady simulations were also performed in the presence of external wind. The rotor was kept in the same position ([0.0, 0.0, 2R]) and the fuselage was not present. The results reported here are related to the condition of advance ratio equal to $\mu = 0.05$. The instantaneous flowfield of the simulation with resolved blades is shown in Figure 10. Also in the presence of external wind, the interaction between helicopter and building is visible. The wake of the rotor limits the development of the recirculation region behind the building [24]. The building in turn, influences the rotor loading, creating asymmetry and inducing oscillations. If the helicopter is in this position, given the characteristics of the two wakes, the higher the advance ratio, the lower the interaction if the helicopter is in this position.

The results of the AD and UAD simulations are presented in Figures 11 and 12, respectively. The non uniform AD model [26] was used for the steady AD computation (the pressure distribution on the rotor disk is reported in Figures 1 (a) and (b)). The input value of C_T in both computations was chosen to correspond to the one obtained with resolved blades simulations, to have a comparison at equal thrust ($C_T = 0.00465$).

Both actuator disk models allow to see the mutual interaction between the two bodies: the existence of the recirculation zone and the asymmetry in the rotor loading are visible. The differences in the instantaneous flowfield between these computation and the fully resolved blades simulation are evident, as we could expect since only the global effect of the rotor is represented. The much slower local vertical velocity is thus explained. This implies that both the AD models do not perturb the flow as much as the blades do and the limits of the recirculation region are not as close to the building. Therefore, both the AD models do not represent the flowfield with enough accuracy. However, it should be noticed that the Unsteady AD technique, for the case tested, achieves better results, since a component of rotational velocity is introduced in the simulation. Instead, the steady AD presents a solution completely symmetric with respect to the xz plane since only the two super-vortices are represented in the wake.

4. WAKE SUPERPOSITION METHOD

The superposition method permits to predict the whole flowfield due to the presence of two bodies by adding directly the two separately computed flows. It consists of simulating the helicopter by means of a simple rotor method (the Actuator Disk in this case) and adding the velocities from a steady or unsteady “frozen” obstacle wake. The overall solution obtained by the superposition method is therefore decoupled, as it neglects the effect that each flowfield causes onto the other. As shown in this work, and already proved in Quinliven and Long [24] and Crozon *et al.* [11], the notion of coupling is important in the context of helicopter operations in “confined areas”. For accurate results, two-way coupled simulations including both obstacle-on-rotor and rotor-on-obstacle effects, are needed. These simulations are computationally expensive, making difficult their use in real time simulators. Therefore, since resolving the flowfield with the superposition method is much cheaper and faster, it is interesting to know when this method can guarantee accurate results and when cannot. The objective is to determine the minimum distance between the helicopter and the building at which the mutual interference can be assumed negligible.

With this purpose, simulations have been computed varying the rotor distance in the building wake (in particular, from 0 to 9 rotor radii away from the leeward edge). The global flowfield obtained by coupled simulations has been compared to the correspondent obtained using the superposition technique. The latter is computed combining point by point the flowfield variables of the two decoupled simulations:

$$p_{\text{Superposition Method}} = \frac{p_{\text{isolated building}} + p_{\text{isolated rotor}}}{2}, \quad (10)$$

$$\rho_{\text{Superposition Method}} = \frac{\rho_{\text{isolated building}} + \rho_{\text{isolated rotor}}}{2} \quad (11)$$

and, since the average velocity U is the same in both simulations,

$$u_{\text{Superposition Method}} = U + u'_{\text{isolated building}} + u'_{\text{isolated rotor}} \quad (12)$$

where u' is the velocity perturbation. All the other variables deriving from pressure, density or velocities (for example, the vorticity) are recomputed using the new variables.

Results for a forward flying rotor at advance ratio of 0.05, are presented in terms of vorticity magnitude, non dimensionnalised by U_∞^2 , in Figure 13. It can be observed that the superposition method guarantees accurate results when the rotor is around $5R$ away from the building. At this distance, therefore, the interference between the two bodies can be assumed negligible. Regarding the loads on the building, the influence of the rotor on the structure vanishes for a distance of about $3R$. Simulations at higher advance ratio, not reproduced here, show similar trends.

5. CONCLUSIONS

This work, within the activity of the *GARTEUR Action Group 22 - “Forces on Obstacles in Rotor Wake”*, studies numerically an helicopter operating in the wake of the building, both in hover and in forward flight. Different aerodynamic

methods were used to represent the rotor: unsteady simulations with fully resolved blades, Actuator Disk and Unsteady Actuator Disk model were performed and the results were compared.

Experimental data from the wind tunnel at the Politecnico di Milano [13] allowed a comparison for the hover case. The agreement of the pressure coefficient distribution on the building and of the flowfield behind the building is overall good and allowed the validation of the CFD flow solver HMB2 [7,31].

Unsteady blades simulations with resolved blades allow for the visualisation of the complex flowfield which results from the interaction between the two aerodynamic wakes. Both the hover and forward flight results show the interaction between the two wakes. Coupled simulations helicopter-building are therefore needed to study this problem, as previous works (see [24] and [11]) have also suggested. The superposition method, which is computationally cheaper to couple the two wakes, has proven to be inaccurate in the case of close proximity between the two bodies. Simulations varying the distance between the building and the rotor modeled as a simple AD showed that the interference effect of the building on the rotor can be assumed negligible when the rotor is at around $5R$ away from it; instead, the building is not effected by the presence of the rotor if the latter is at a distance greater than $3R$.

Coupled unsteady simulations with the Actuator Disk method shows the existence of the interaction but are not able to capture the phenomenon with sufficient accuracy. The rotor in the AD models is represented only via its integral effect and the effect of the rotation of the blades is not taken into account. The unsteadiness of the phenomenon is not captured accurately and the resulting flowfield is symmetric, since the method models only the two super-vortices of the wake but not the individual blade vortices.

The Unsteady Actuator Disk model is a hybrid technique derived from the Actuator Line [27] and mimics the presence of the blades by shaping the load distribution on the disk using a Gaussian function. Results showed better agreement with simulations with resolved blades since the effect of the blades rotation is partially taken into account. However, also this method does not show the complexity of the flowfield that generates from the interaction between the two wakes.

It should be noticed that the UAD simulation presents some difficulties compared to the simple AD, due to the need of to localise the cells that belong to the blade at each time step. However, the computational time of the UAD and AD methods are comparable and are computationally cheaper than simulations with fully resolved blades. An improvement of this technique can therefore become the most efficient aerodynamic model to study this phenomenon.

6. FUTURE WORK

Future work seeks to investigate in more detail the effect of the interaction between helicopter and building, both from the point of view of the rotorcraft and of the structure. First, simulations fully resolving the blades including a ROBIN model of the fuselage are to be carried out to evaluate any fuselage

effects. The results could also help in the explanation of the asymmetry registered in the experiments in POLIMI. Besides, to better comprehend the effect of the flowfield on the rotor, unsteady simulations including a trimmer can be performed. The results of these simulations can be compared with the result of multi-body dynamic code (for example FlightLab [3]) in which the “frozen” obstacle wake can be introduced before. Finally, different position of the helicopter can be analysed (a configuration with the rotorcraft windward or in a lateral position with respect to the building can be interesting) and the effect of the relative dimensions rotor-building can be also studied.

The UAD model can also be improved introducing a different kernel function to better simulate the real radial distribution of the blade loading.

Regarding the building, a more detailed study of the pressure coefficient distribution will be carried out, analysing the accuracy of the AD models. Besides, future experiments within the AG22 will provide unsteady pressure distribution on the obstacle and a comparison could be made. An analysis of the loads spectrum it is interesting to investigate also if the unsteady actuator disk model reproduces the blades passing. Finally, the effect of rounded edges around the building should be studied.

7. ACKNOWLEDGEMENTS

The use of the data of the experiments by Gibertini *et al.* [13] is gratefully acknowledged.

REFERENCES

- [1] Ansys icem cfd.
<http://www.ansys.com/Products/Other+Products/ANSYS+ICEM+CFD/>.
Last visit: 10/04/2015.
- [2] Aviation accident reports - national transportation safety board.
<http://www.ntsb.gov/investigations/AccidentReports/Pages/aviation.aspx>.
Last visit: 10/04/2015.
- [3] Flightlab - advanced rotorcraft technology inc.
<https://www.flighthlab.com/flighthlab.html>.
Last visit: 10/04/2015.
- [4] International helicopter safety team.
<http://www.ihst.org/>.
Last visit: 21/04/2015.
- [5] Wind history in liverpool.
<http://www.wunderground.com/history/>.
Last visit: 21/04/2015.
- [6] O. Axelsson. *Iterative Solution Methods*. Cambridge University Press, Cambridge, MA, edition, 1994.
- [7] G.N. Barakos, R. Steijl, K. Badcock, and A. Brocklehurst. Development of cfd capability for full helicopter engineering analysis. *31th European Rotorcraft Forum*, 2005.
- [8] M. Behr. ROBIN Fuselage.
<http://www.cats.rwth-aachen.de/library/research/technotes>.
Last visit: 10/04/2015.
- [9] J. Boussinesq. *Théorie de l’Écoulement Tourbillonant et Tumultueux des Liquides dans des Lits Rectilignes à Grande Section, Tome I-II*. Gauthier-Villars, Paris, France, first edition, 1897.
- [10] B. Cabral and L.C. Leedom. Imaging vector fields using line integral convolution. *20th Annual Conference and Exhibition on Computer Graphics and Interactive Techniques - Anaheim, CA, USA*, 1993.
- [11] C. Crozon, R. Steijl, and G.N. Barakos. Numerical study of helicopter rotors in a ship airwake. *Journal of Aircraft*, 51:1813–1832, 2014.
- [12] A. Fradenburgh. The helicopter and the ground effect machine. *Symposium on Ground Effect Phenomena, Princeton University*, 1959.
- [13] G. Gibertini, D. Grassi, C. Parolini, D. Zagaglia, and A. Zanotti. Experimental investigation on the aerodynamic interaction between a helicopter and ground obstacles. *Journal of Aerospace Engineering*, 2014.
- [14] M. Jarwowsky, M.A. Woodgate, G. Barakos, and J. Rokicki. Towards consistent hybrid overset mesh methods for rotorcraft cfd. *International Journal for Numerical Methods in Fluids*, 74:543–576, 2014.
- [15] J. Jeong and F. Hussain. On the identification of a vortex. *Journal of Fluid Mechanics*, 285, 1995.
- [16] S.J. Lawson, M. Woodgate, R. Steijl, and G.N. Barakos. High Performance Computing for Challenging Problems in Computational Fluid Dynamics. *Progress in Aerospace Sciences*, 52:19–29, July 2012.
- [17] J.G. Leishman. *Principles of Helicopter Aerodynamics*. Cambridge University Press, 2006.
- [18] T. Lusiak, A. Dziubinski, and K. Szumanski. Interference between helicopter and its surroundings, experimental and numerical analysis. *Task Quarterly* 13, 2010.
- [19] F.R. Menter. Two-Equation Eddy-Viscosity Turbulence Models for Engineering Applications. *AIAA Journal*, 32(8):1598–1605, August 1994.
- [20] F.R. Menter and Y. Egorov. A Scale Adaptive Simulation Model using Two-Equation Models. *43rd AIAA Aerospace Sciences Meeting and Exhibit*, 2005.
- [21] S. Osher and S. Chakravarthy. Upwind Schemes and Boundary Conditions with Applications to Euler Equations in General Geometries. *Journal of Computational Physics*, 50:447–481, January–February 1983.
- [22] J.-B. Paquet, J.-P. Bourez, and S. Morgand. Formulation of aerodynamic forces on helicopters in non uniform flow with scale model tests: Ground effects. *3AF - 49th International Symposium of Applied Aerodynamics*, 2014.

- [23] S.A. Polksy and C.H. Wilkinson. A computational study of outwash for a helicopter operating near a vertical face with comparison to experimental data. In *AIAA Modeling and Simulation Technologies Conference 10-13 August 2009, Chicago, Illinois*, AIAA 2009-5684, 2009.
- [24] T. A. Quinlivan and K. R. Long. Rotor performance in the wake of a large structure. *American Helicopter Society, 65th Annual Forum*, 2009.
- [25] F. Rieper. A low-mach number fix for roe's approximate riemann solver. *Journal of Computational Physics*, 230:5263–5287, 2011.
- [26] V.I. Shaidakov. Disk vortex theory of main rotor with constant loading on the disk. *Helicopter Designs Aerodynamics*, 1976.
- [27] J. N. Sorensen and W. Z. Shen. Numerical modeling of wind turbines wakes. *Journal of Fluids Engineering*, 136, 2002.
- [28] Ph. Spalart. Strategies for Turbulence Modelling and Simulations. *International Journal of Heat and Fluid Flow*, 21(3):252–263, June 2000.
- [29] Ph. Spalart and S.R. Allmaras. A One-Equation Turbulence Model for Aerodynamic Flows. *La Recherche Aérospatiale*, 1:5–21, 1994.
- [30] R. Steijl and G. Barakos. Sliding mesh algorithm for cfd analysis of helicopter rotor-fuselage aerodynamics. *International Journal for Numerical Methods in Fluids*, 58:527–549, 2008.
- [31] R. Steijl, G. Barakos, and K. Badcock. A framework for cfd analysis of helicopter rotors in hover and forward flight. *International Journal for Numerical Methods in Fluids*, 51(8):819–847, 2006.
- [32] G.D. van Albada, B. van Leer, and W.W. Roberts, Jr. A comparative study of computational methods in cosmic gas dynamics. *Astronomy and Astrophysics*, (108):76–84, 1982.
- [33] B. van Leer. Flux-vector splitting for the euler equations. In *Eighth International Conference on Numerical Methods in Fluid Dynamics*, volume 170 of *Lecture Notes in Physics*, pages 507–512. Springer Berlin / Heidelberg, 1982.
- [34] D.C. Wilcox. Multiscale Model for Turbulent Flows. *AIAA Journal*, 26(11):1311–1320, November 1988.

Tables

Grid ID	Sub-Grids	Geometry	N° of Blocks	N° of Cells [million]	Dedicated CPUs
G1		AD/UAD rotor only	96	5.1	12
G2		single blade IGE	442	7.3	64
		single blade OGE	618	8.5	64
G3		building only	1139	10.1	8
G4	G-a, G-b, G-c	building + AD/UAD rotor	135	12.6	48
G5	G-a, G-d, G-e, G-c	building + rotor with blades	2014	28.7	128
G6	G-a2, G-f, G-g, G-h, G-c	building + rotor with blades + fuselage	2044	33.6	128

Table 1: Computational grids of the final simulations.

Sub-Grid ID	Geometry	N° of Blocks	N° of Cells [million]
G-a	building	66	5.4
G-a2	building	229	5.5
G-b	AD background	58	7.1
G-c	external background	11	0.2
G-d	complete rotor 1	1856	21.5
G-e	rotor background	81	1.6
G-f	complete rotor 2	1328	22.4
G-g	fuselage	476	5.6
G-h	helicopter background	11	0.1

Table 2: Computational sub-grids.

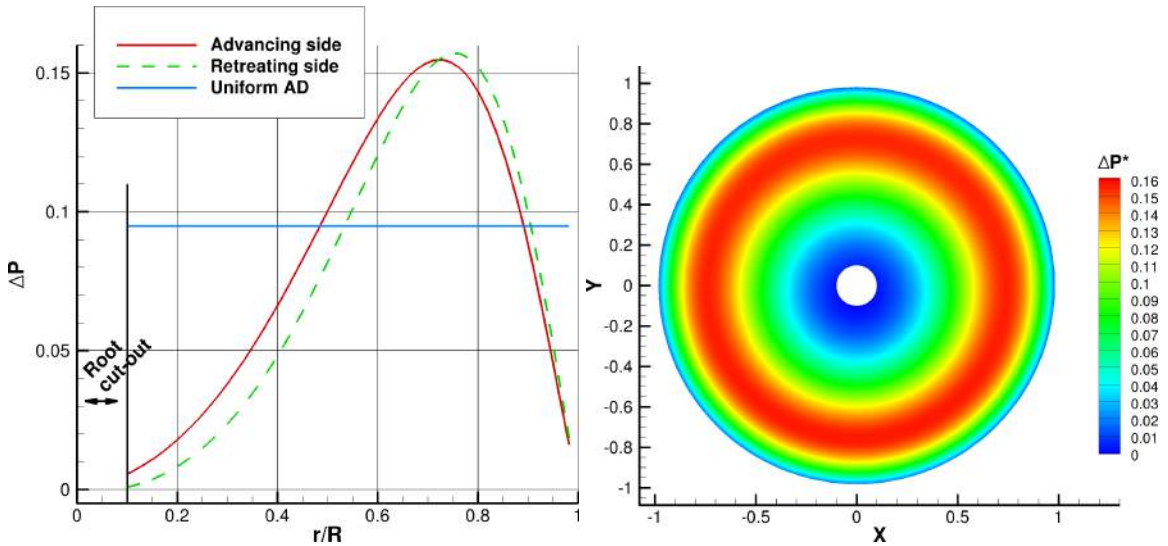
	Rotor on the Building Edge	Rotor In Ground Effect
C_T	0.0063	0.0131

Table 3: Thrust coefficient of the helicopter in hover above the edge of the building ($0.8R$ from the building roof) and comparison with the IGE simulation at $0.8R$ above the ground.

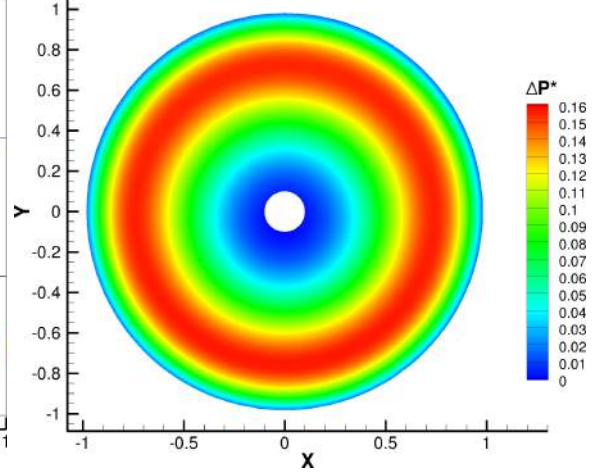
	Thrust Coefficient	Torque Coefficient	Figure of Merit
“Numerical Rotor”	0.0107	0.000884	0.625
Helicopter Model	0.0137	0.00146	0.561

Table 4: Comparison between performance indices of the helicopter of the experiments in POLIMI (test 1 of [13]) and the numerical simulation with fully resolved blades.

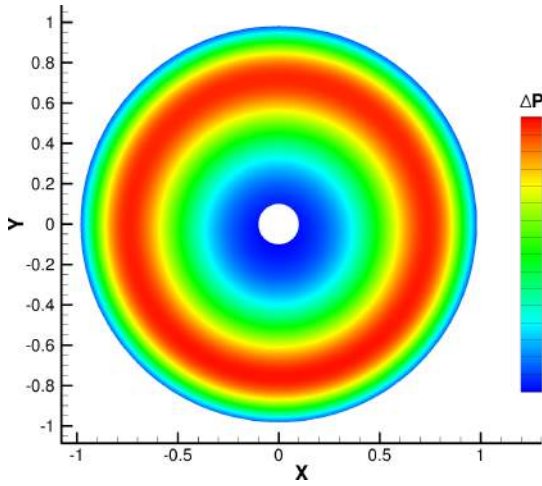
Figures



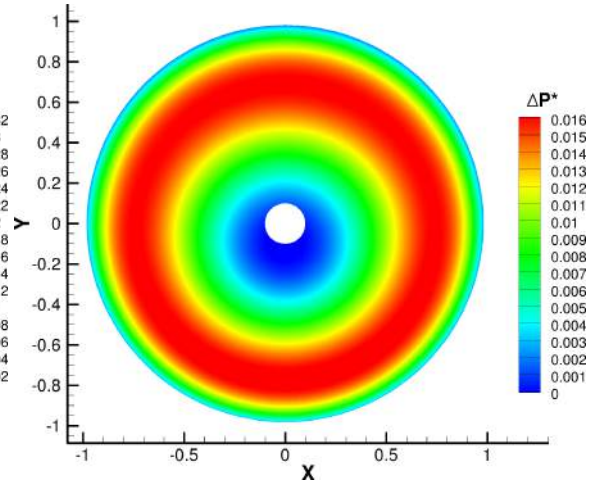
(a) Pressure jump distribution as a function of the radial coordinate for advancing ($\Psi = 90 \deg$) and retreating ($\Psi = 270 \deg$) side - $\mu = 0.05$ and $C_T = 0.00465$.



(b) Non dimensional pressure jump distribution across the disk for $\mu = 0.05$ and $C_T = 0.00465$.

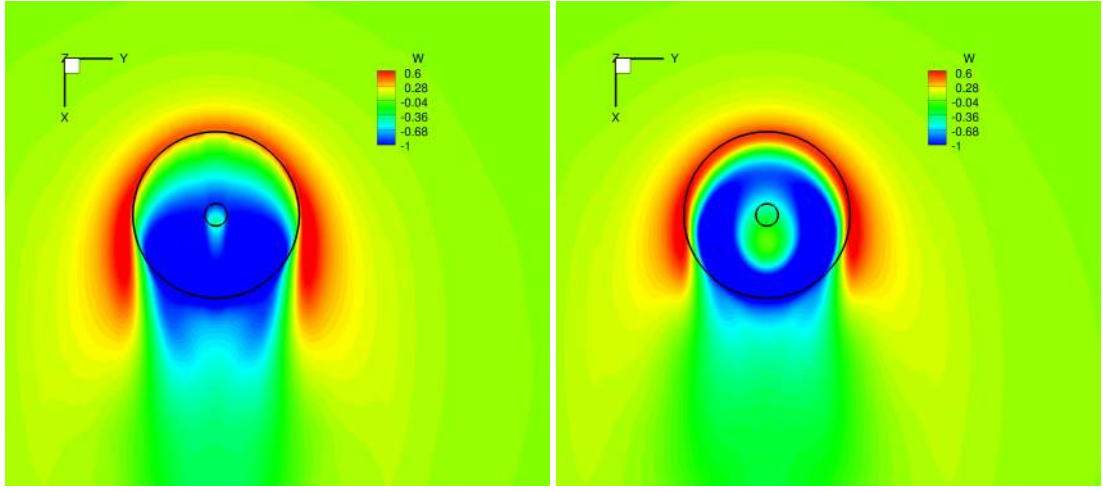


(c) Non dimensional pressure jump distribution across the disk at higher C_T - $\mu = 0.05$ and $C_T = 0.009$.



(d) Non dimensional pressure jump distribution across the disk at higher advance ratio - $\mu = 0.15$ and $C_T = 0.00465$.

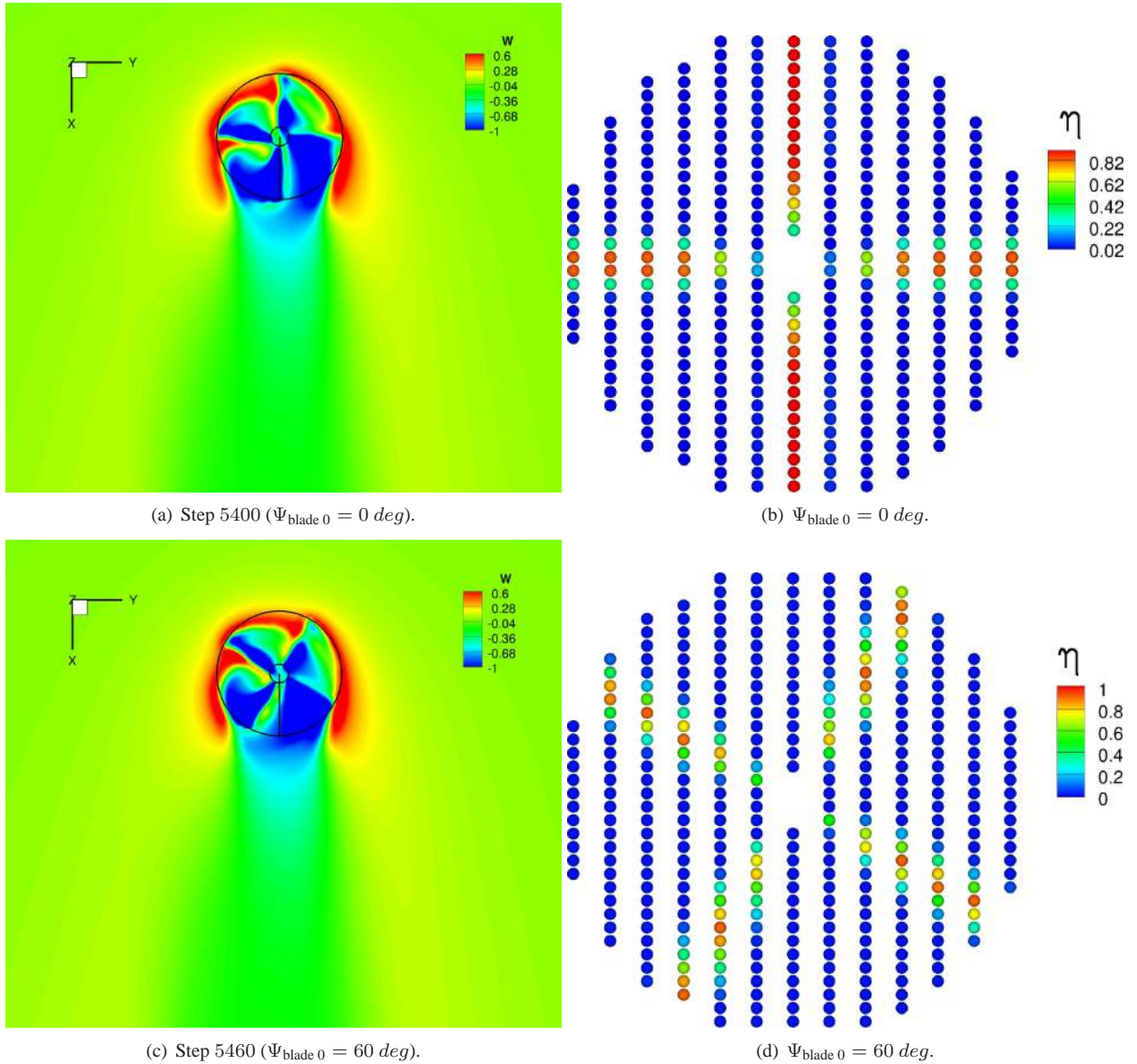
Figure 1: Non uniform Actuator Disk [26] model in HMB2. Pressure distribution (wind parallel to the x axis, positive in the positive direction of this) for different thrust coefficient and advance ratio. The model assumes a symmetric loading with respect to the direction perpendicular to the wind, different for the advancing and the retreating side.



(a) Uniform Actuator Disk.

(b) Non uniform Actuator Disk [26].

Figure 2: Actuator Disk models in HMB2. Vertical velocity distribution in the plane of the disk ($\mu = 0.05$, $C_T = 0.022$).



(a) Step 5400 ($\Psi_{blade\ 0} = 0\ deg$).

(b) $\Psi_{blade\ 0} = 0\ deg$.

(c) Step 5460 ($\Psi_{blade\ 0} = 60\ deg$).

(d) $\Psi_{blade\ 0} = 60\ deg$.

Figure 3: Unsteady Actuator Disk model implemented in HMB2. Vertical velocity distribution in the plane of the disk ($\mu = 0.05$, $C_T = 0.0092$) at two different time steps of the simulation, on the left, and the correspondent Actuator disk showing as red points the cells contained in the blade, on the right.

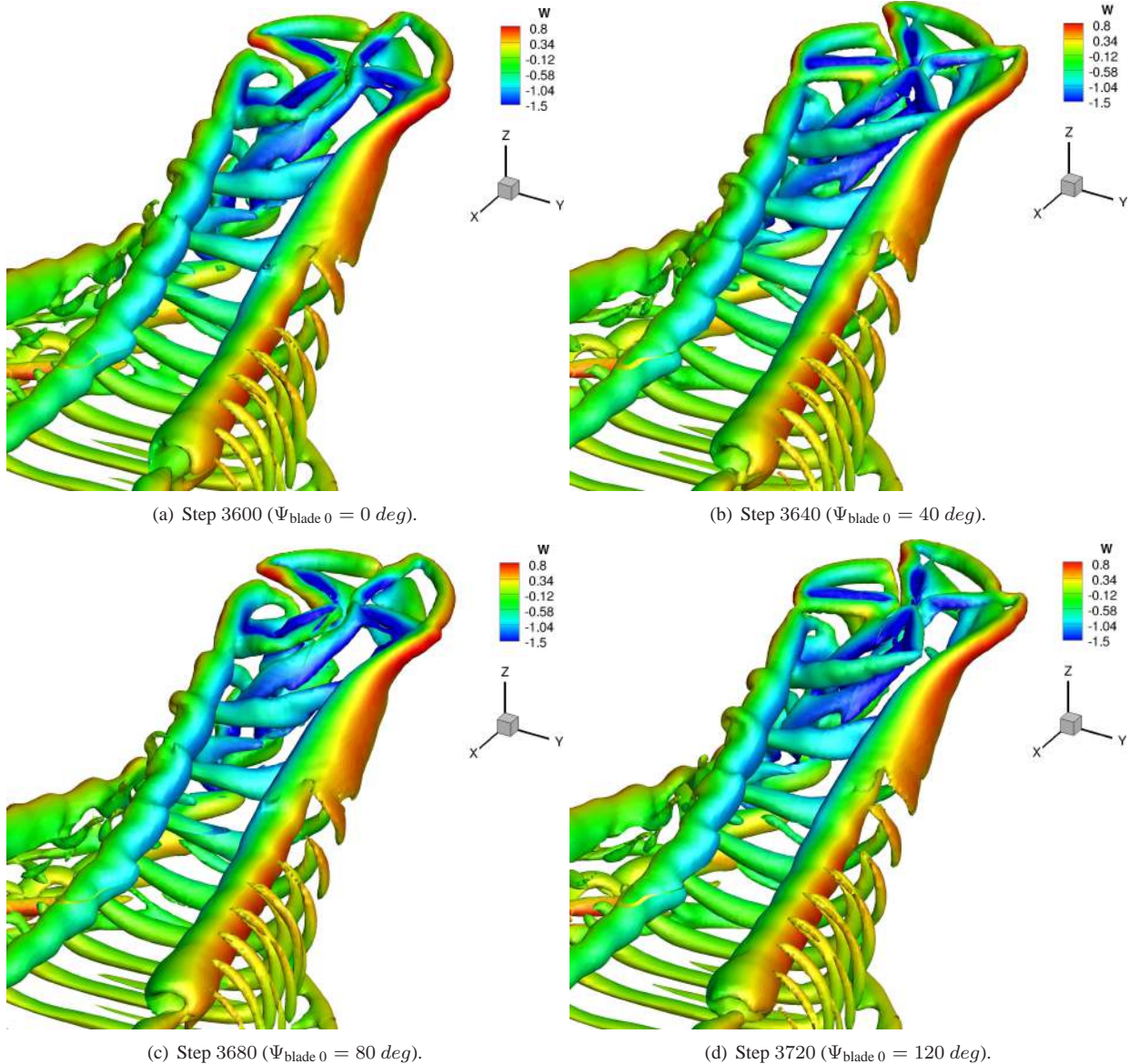
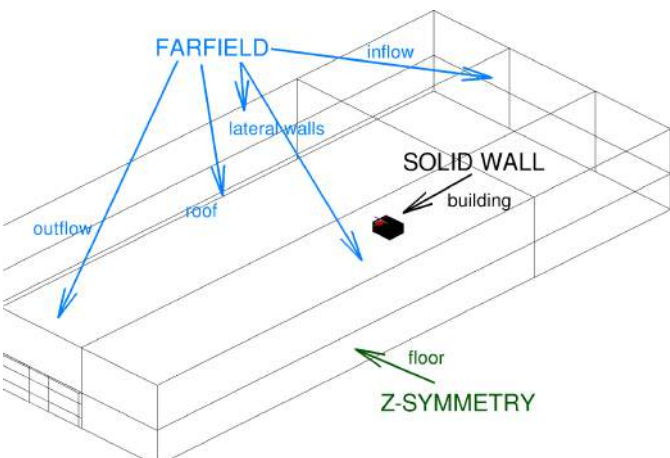
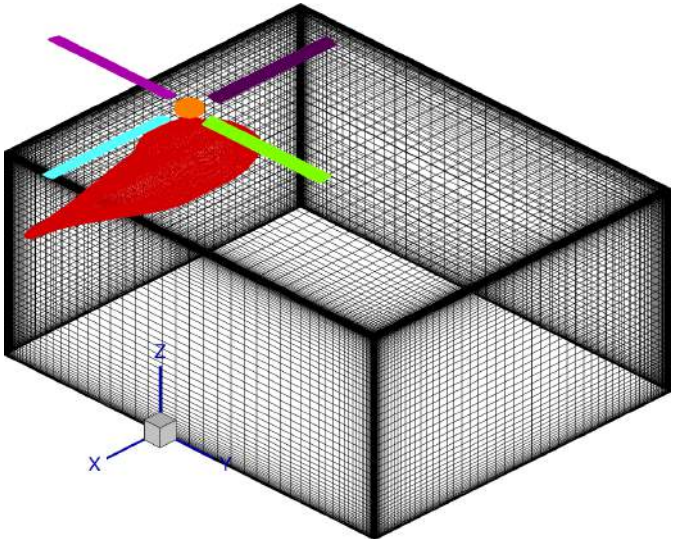


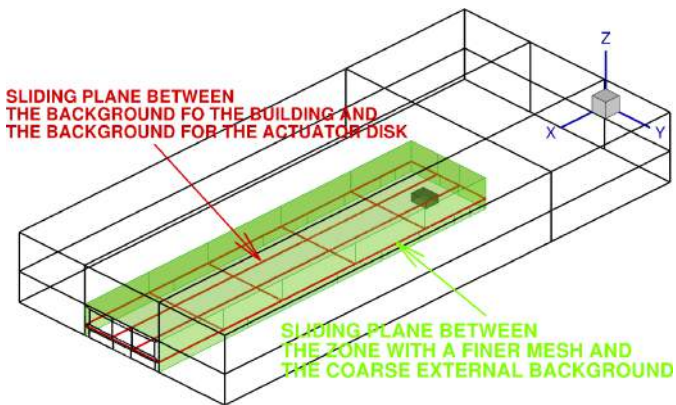
Figure 4: Unsteady Actuator Disk model implemented in HMB2. Wake vortical structures visualisation ($\mu = 0.05$, $C_T = 0.0092$) at different time steps of the simulation. Isosurfaces of Q [15] colored with the vertical velocity component.



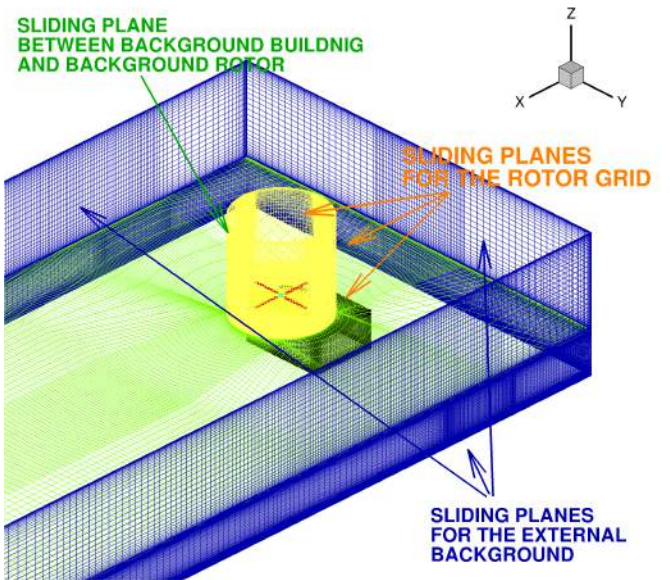
(a) Full computational domain with boundary conditions applied to the problem.



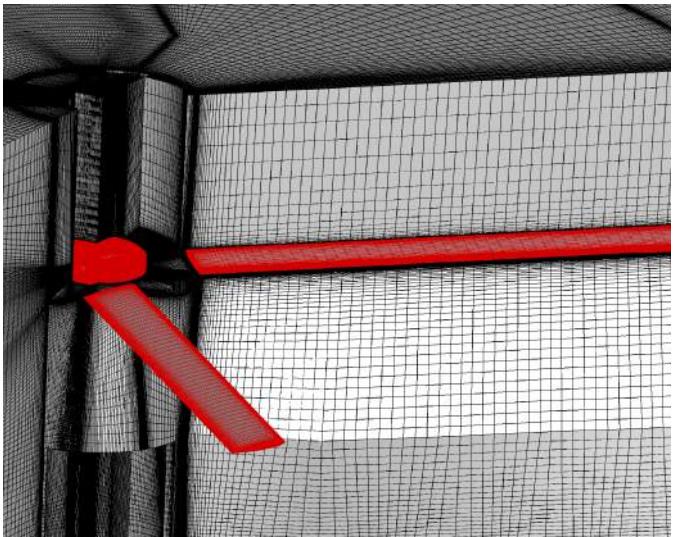
(b) Detail of the building and the helicopter with the definition of the frame of reference.



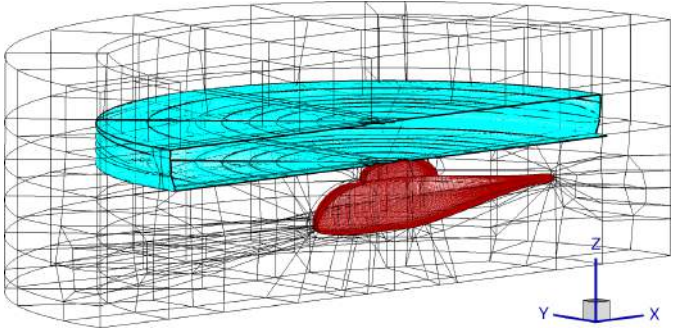
(c) Structure of the assembled grid for the coupled simulations with the rotor modeled as an Actuator Disk (G4). View of the full computational domain.



(d) Structure of the assembled grids of the coupled problem with fully resolved blades (grid G5). Detail of the building and the rotor.

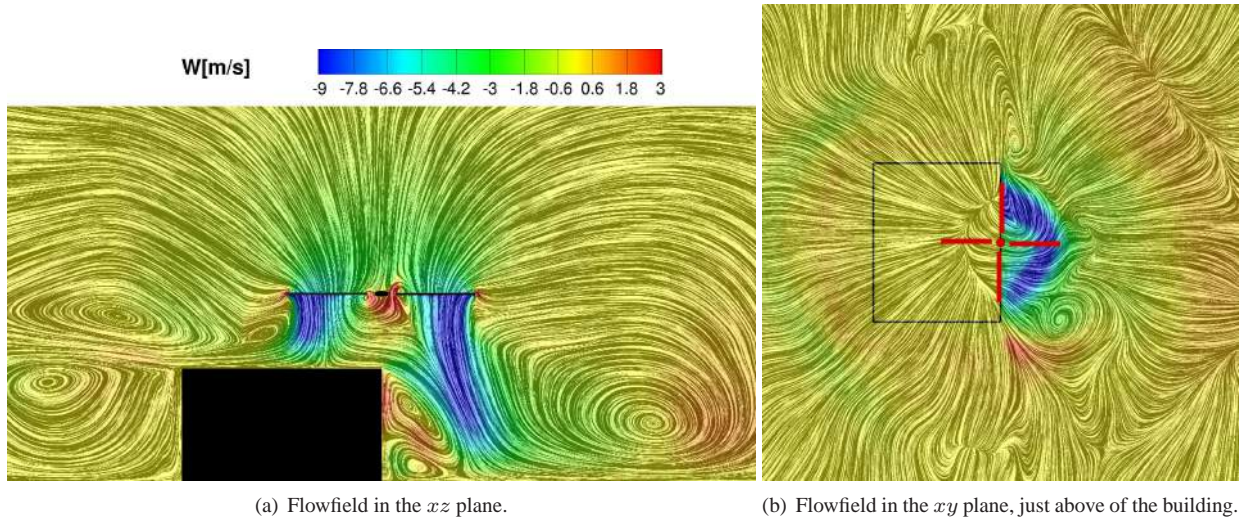


(e) Detail of the mesh of the rotor grid (grid G-d). A C-mesh is used around the blade and this is included in a larger H structure which fills up the rest of the computational domain. A more detailed description of the multi-block topology used can be found in Steijl *et al.* [31].



(f) Topology of the CHIMERA [14] grid (grid G-g) to simulate the complete helicopter. Detail of the fuselage mesh and of the drum for the rotor grid (surface of the sliding planes in blue). Only half of the grid has been generated and then mirrored, ensuring a perfect symmetry.

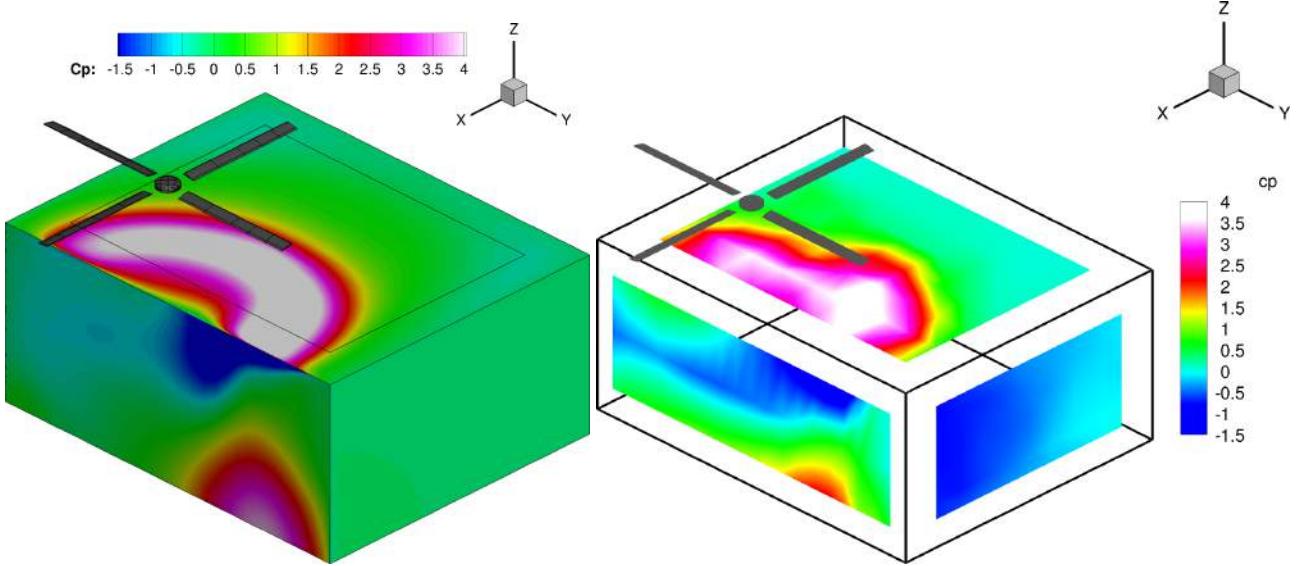
Figure 5: Computational grid details. Dimensions, in terms of number of cells and CPUs, are reported in Tables 1 and 2.



(a) Flowfield in the xz plane.

(b) Flowfield in the xy plane, just above of the building.

Figure 6: Full-blades simulation for hover with the rotor laying on the building edge at a distance of one diameter above the ground. Instantaneous flowfield (18^{th} rotor revolution, $\Psi_{\text{blade}0} = 0 \deg$), visualised via the Linear Integral Convolution method [10], colored with the vertical velocity component.



(a) Numerical simulation results, averaged on the 17^{th} rotor revolution. (b) Experimental data (test 5.2 of [13]), averaged over 10 observation seconds.

Figure 7: Pressure coefficient distribution on the building for hover with the rotor at a distance of one diameter above the ground and with its center laying exactly on the building edge.

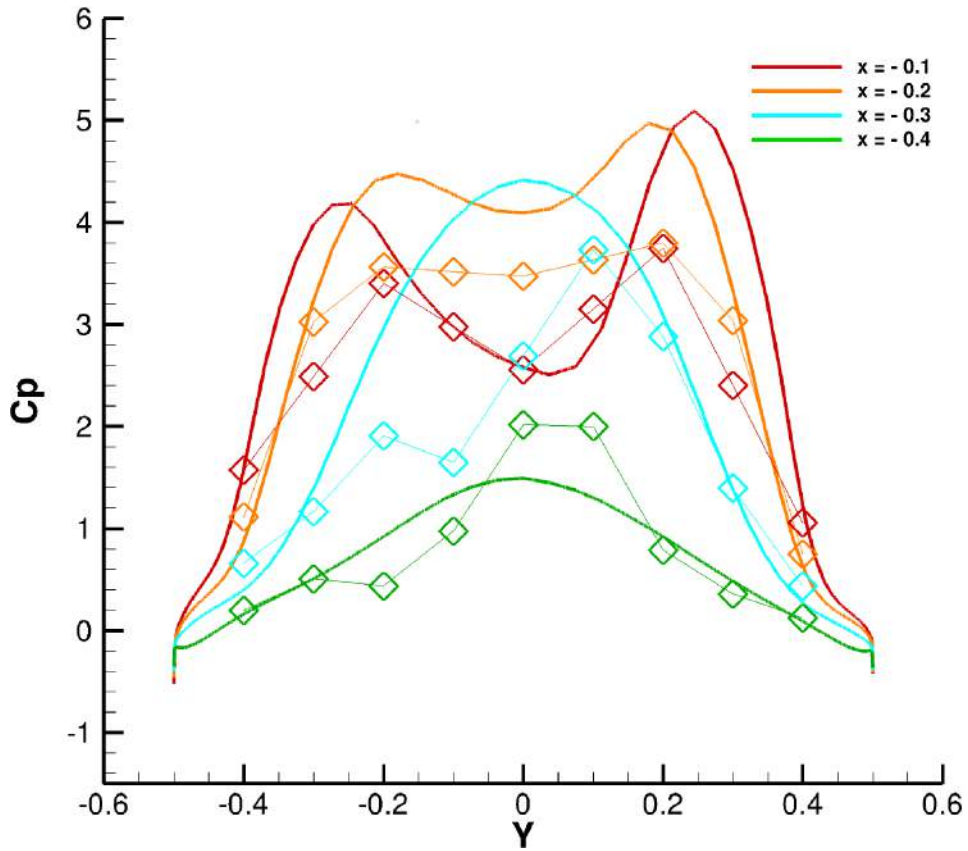


Figure 8: Comparison of the pressure coefficient distribution on the top face of the building for hover with the rotor at a distance of one diameter above the ground and with its center laying exactly on the building edge. Full-blade simulation results averaged on the 17th rotor revolution vs experimental data (test 5.2 of [13]) averaged over 10 observation seconds.

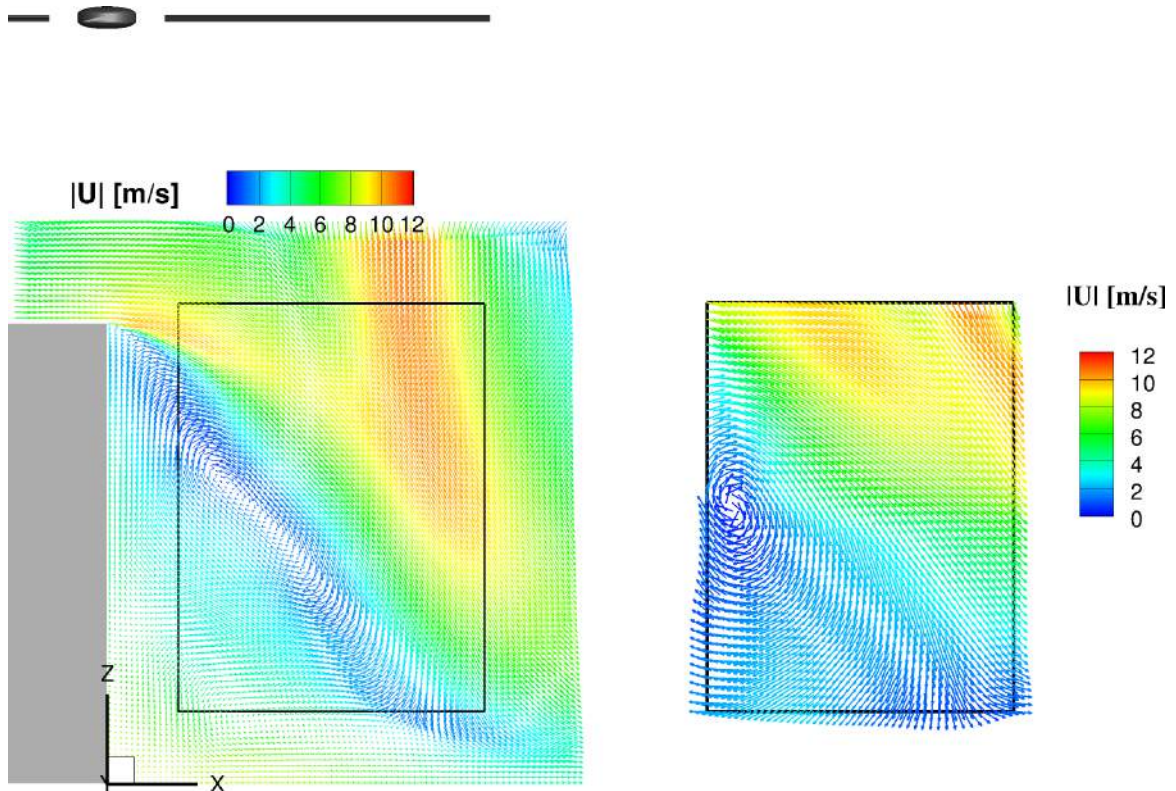


Figure 9: Flowfield behind the building on the symmetry plane for hover with the rotor at a distance of one diameter above the ground and with its center laying exactly on the building edge. Comparison between CFD results and experimental data (test 5.2 of [13]). On the left, full-blades simulation results averaged on the 17th rotor revolution. On the right, experimental data, averaged over 10 observation seconds.

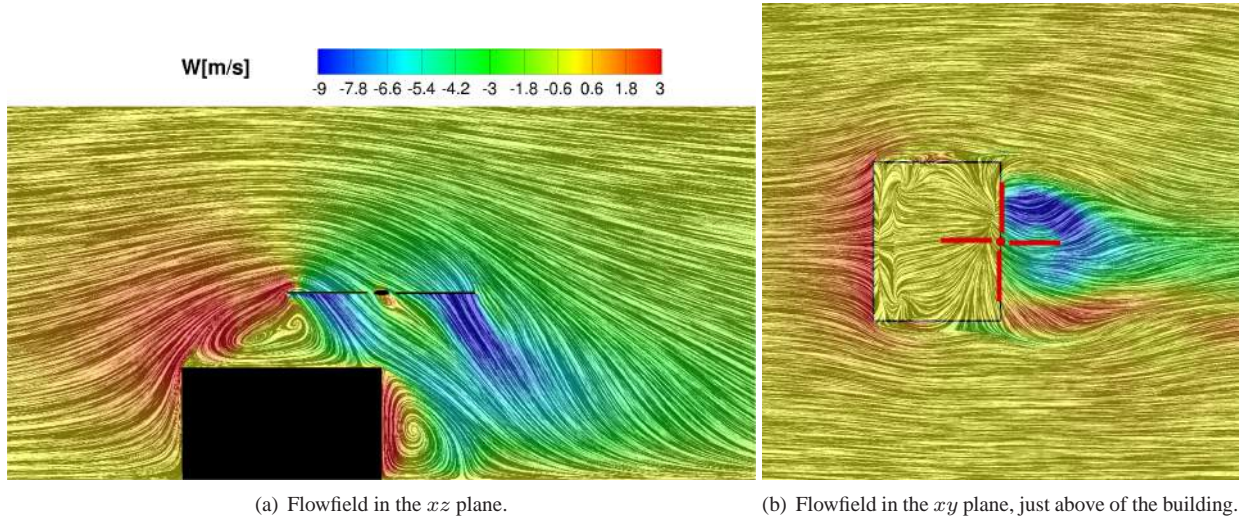


Figure 10: Full-blades simulation for forward flight rotor at $\mu = 0.05$ on the building leeward edge at a distance of one diameter above the ground. Instantaneous flowfield (19^{th} rotor revolution, $\Psi_{\text{blade } 0} = 0 \deg$), visualised via the Linear Integral Convolution method [10], colored with the vertical velocity component.

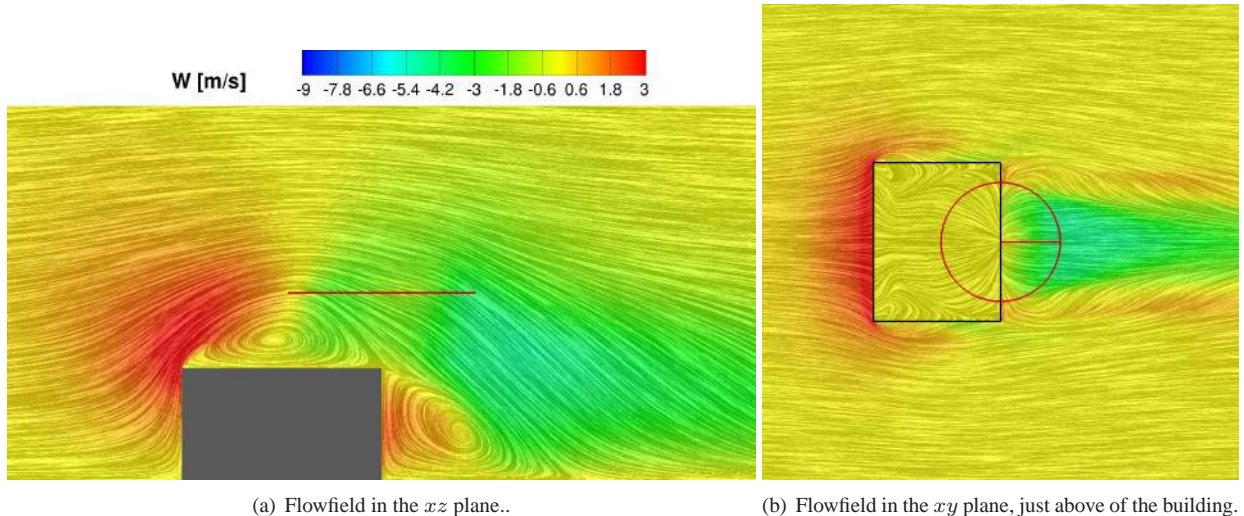
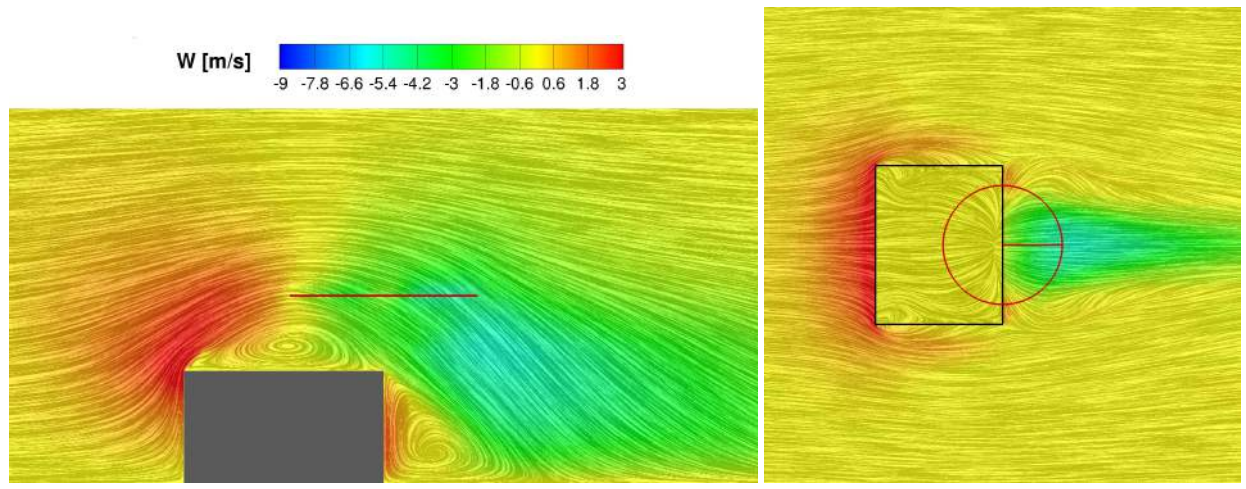


Figure 11: AD simulation for forward flight rotor at $\mu = 0.05$ on the building leeward edge at a distance of one diameter above the ground. Instantaneous flowfield (after 6 full rotor revolution), visualised via the Linear Integral Convolution method [10], colored with the vertical velocity component.



(a) Flowfield in the xz plane.

(b) Flowfield in the xy plane, just above of the building.

Figure 12: UAD simulation for forward flight rotor at $\mu = 0.05$ on the building leeward edge at a distance of one diameter above the ground. Instantaneous flowfield (after 9 full rotor revolution), visualised via the Linear Integral Convolution method [10], colored with the vertical velocity component.

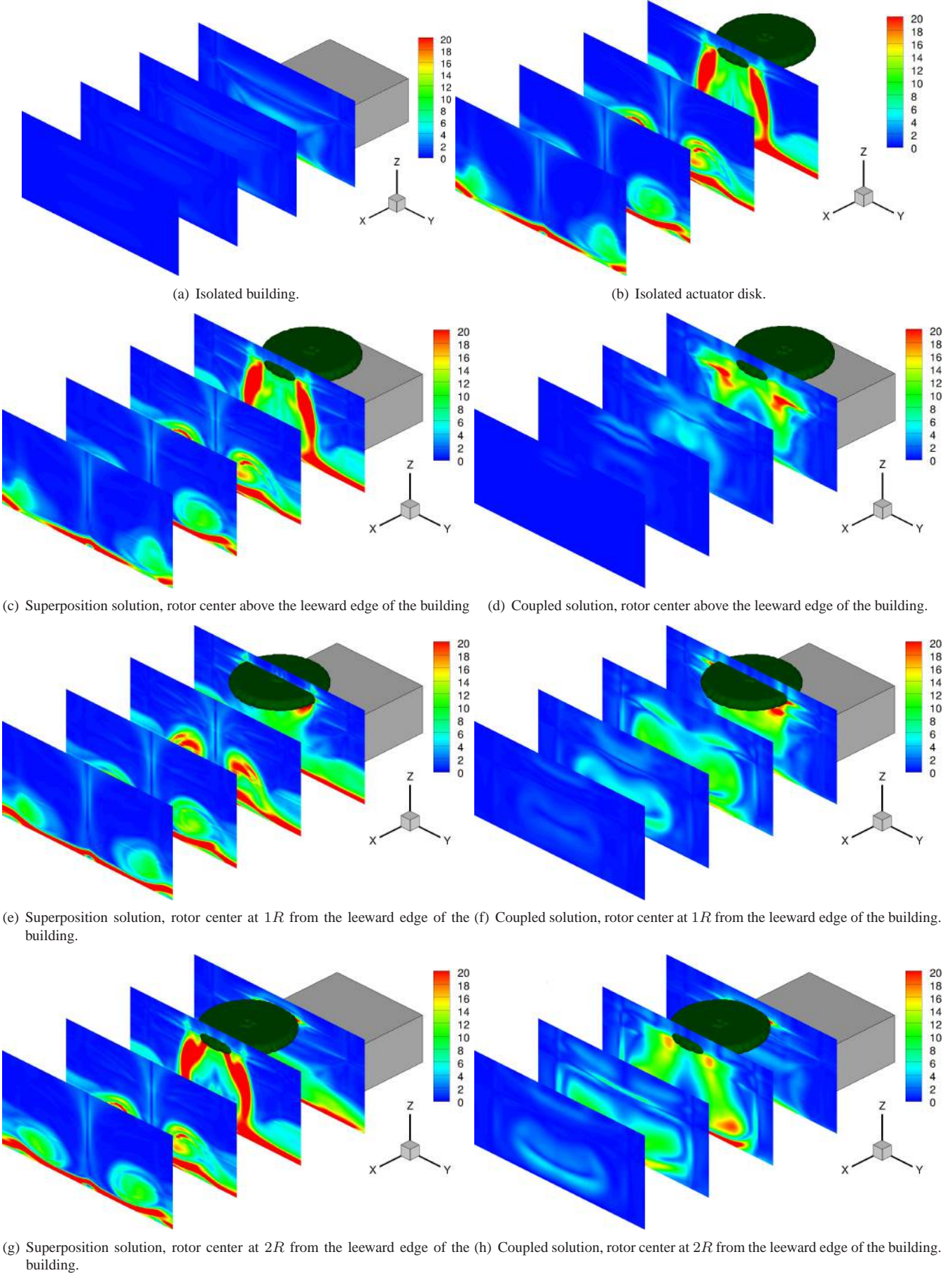


Figure 13: Analysis of the Superposition Method. Maps of vorticity, non dimensionalised by U_∞^2 . Rotor advance ratio $\mu = 0.05$, $M_\infty = 0.0143$. The rectangular zone selected for the analysis begins around one length before the building and covers the flowfield until 10 building lengths downstream and it is discretised using $75 \times 75 \times 75$ points.

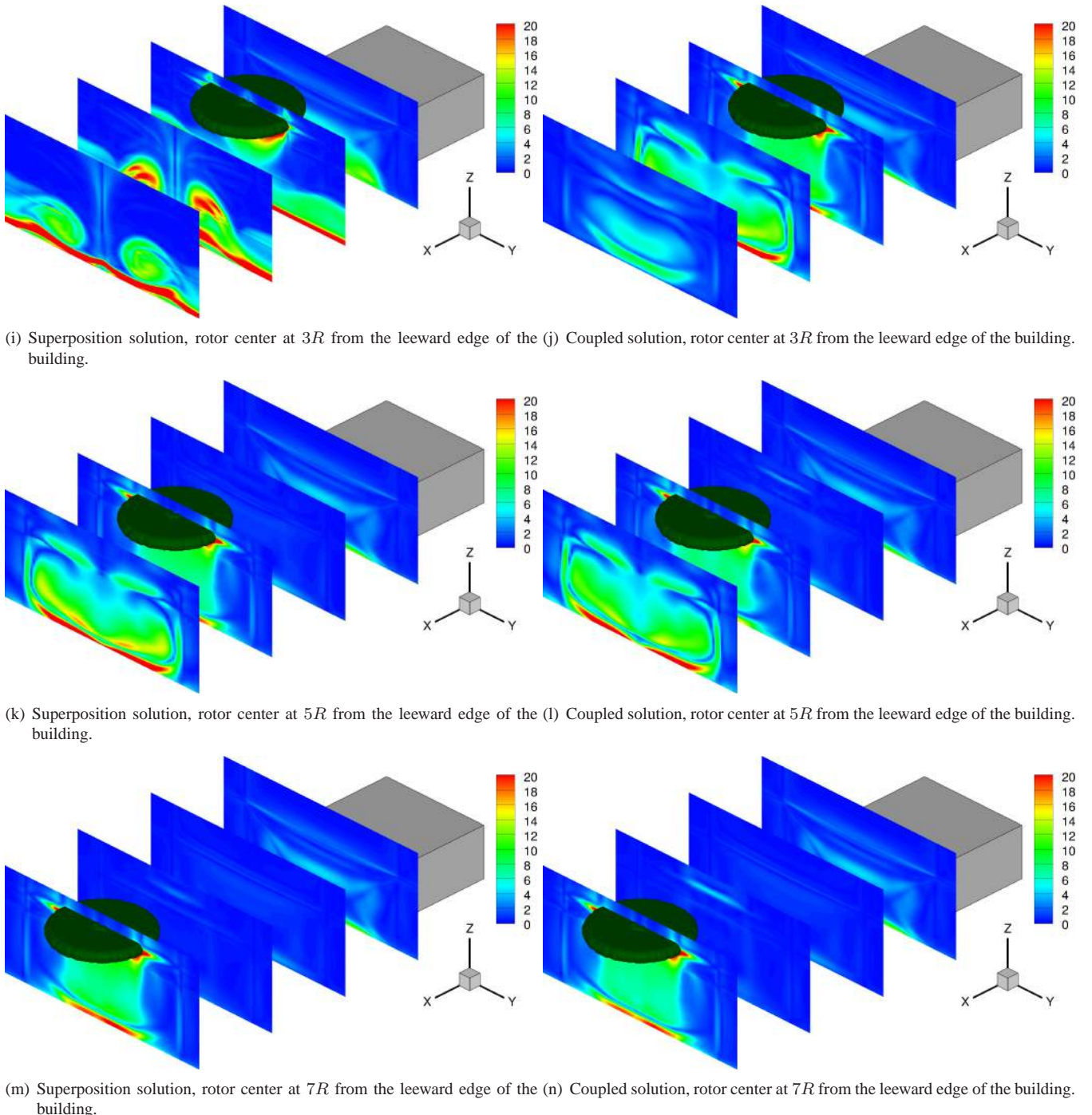


Figure 13: *continued* - Analysis of the Superposition Method. Maps of vorticity, non dimensionalised by U_∞^2 . Rotor advance ratio $\mu = 0.05$, $M_\infty = 0.0143$. The rectangular zone selected for the analysis begins around one length before the building and covers the flowfield until 10 building lengths downstream and it is discretised using $75 \times 75 \times 75$ points.